Lab on a Chip

Devices and applications at the micro- and nanoscale

Accepted Manuscript

This article can be cited before page numbers have been issued, to do this please use: A. Mercader, S. Ye, W. R. Wagner and S. K. Cho, *Lab Chip*, 2026, DOI: 10.1039/D6LC00360E.

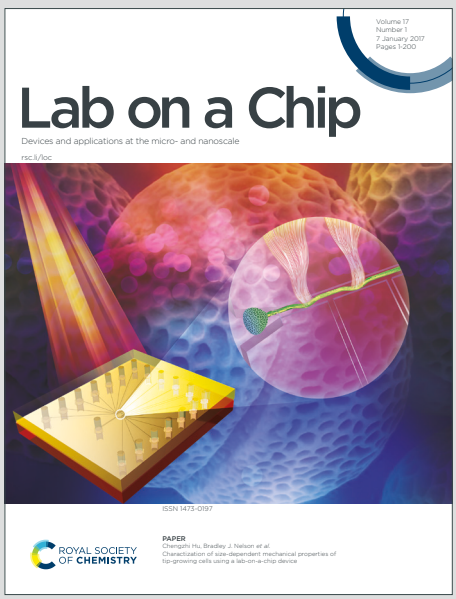

ROYAL SOCIETY OF CHEMISTRY

rsc.li/loc

View Article Online
DOI: 10.1039/D6LC00360E

ARTICLE

Improved Oxygenation and Hemocompatibility for Microfluidic Artificial Lung via Membrane Microstreaming

Anthony Mercader‡[a], Sang-Ho Ye [b], William R. Wagner [b] and Sung Kwon Cho* [c]

Received 00th January 20xx,
Accepted 00th January 20xx

DOI: 10.1039/x0xx00000x

Microfluidic artificial lung devices seek to capitalize on the increased surface area to volume ratio of the micro scale to increase gas exchange efficiency, allowing for oxygenation of blood with smaller volumes and a smoother flow path. However, such small scales also lead to challenges including coagulation and channel blockage and difficulty in scaling up. This article presents the integration of active mixing to the blood side channel via acoustic microstreaming by an oscillating membrane to enhance gas exchange across that membrane. Tests with fresh ovine blood show reduced biofouling by platelet deposition on the actuated membranes (up to 80% lower surface coverage), which may extend device lifetimes. Coagulation and channel blockage experiments demonstrate reduced coagulation of and channel blockage in taller and actuated channels. O_2 gas exchange into ovine blood is improved up to 2.6x compared to the non-actuated control, allowing blood pumped through the device to reach a 95% target for oxygen saturation with channel geometry and flow parameters which would be otherwise unsuitable. Such a design allows for taller channel heights than are typically seen in microfluidic artificial lung devices while maintaining gas exchange efficiency, enabling the device to capitalize on the reduced coagulation associated with the taller, actuated channels, enabling easier fabrication by conventional machining, and allowing for larger throughput per channel branch.

Introduction

The microfluidic artificial lung in concept is an evolution of the existing Extracorporeal Membrane Oxygenator (ECMO), a medical device which serves to oxygenate blood in patients with limited lung functionality by flowing blood out of the body and across a bundle of hollow fibers perfused with oxygen. The microfluidic version seeks to take advantage of scaling laws by miniaturizing the blood flow and gas-permeable membrane to improve gas exchange efficiency due to the increased surface-area-to-volume ratio, as mass transfer is limited by diffusion in the strictly laminar flow. These devices typically take the form of a microchannel for blood flow separated from a gas channel by a permeable polydimethylsiloxane (PDMS) membrane [1].

Such devices face several challenges when attempting to push the technology towards commercialization and medical use, including throughput and long-term hemocompatibility [1, 2]. For throughput, it is natural that although scaling down the channel size will increase gas exchange efficiency due to the increased surface area to volume ratio, it is challenging to develop a device with enough total gas transfer area to support clinical needs, since each individual channel branch must be small. To address this, research is ongoing to scale up a single channel or branching paths by combining multiple layers in parallel [3], or by creating designs with intrinsically more surface area for gas exchange [4]. These devices may also be more suitable for neonatal lung assistance, for example, as the requirement for total throughput will naturally be much lower, and scaling up to that level may be more feasible [5]. For hemocompatibility, reducing the size of the channel the blood must flow through greatly increases the shear stress experienced by the fluid and exposure to foreign surfaces, often triggering a coagulation response, fouling of the channel surface, and blockage [6]. In fact, for a constant flow rate, the shear is scaled to the 3rd power with decreasing side length for a constant aspect ratio, an extreme trade-off between efficiency and hemocompatibility.

In many microfluidic artificial lungs, channel heights may be as small as 10 μm, close to the diameter of an individual red blood cell. Careful optimization is required to find ideal dimensions, and there is much work to reduce the shear experienced by the blood. For one, the details of the branching geometry can be carefully designed to mimic that seen in biology to provide the smoothest possible flow path [7]. Also, the materials used to form the channels have been modified to reduce shear by both surface and volume modifications [8-10]. Nonetheless, the scaling of shear stress with channel dimension and increased foreign contact surface area leaves it highly desirable to allow for larger channel dimensions if it is possible to maintain equivalent gas transfer efficiency. This work studies the application of active mixing to the liquid channel in order to improve the gas transfer efficiency using larger channel heights,

[a] Department of Mechanical Engineering and Materials Science, University of Pittsburgh, Pittsburgh, PA 15261, USA.
[b] Department of Bioengineering, University of Pittsburgh, Pittsburgh, PA 15261, USA.
[c] Department of Mechanical Engineering and Materials Science, University of Pittsburgh, Pittsburgh, PA 15261, USA. E-mail: skcho@pitt.edu
*Corresponding Author
‡Current address: University of Illinois Urbana-Champaign, Urbana, IL 61801, USA
† AM and SHY make equal contributions to this paper.
Supplementary Information available: X

alleviating shear and contact surface allowing for larger throughput through an individual channel.

The low Reynolds number laminar flow seen at these microchannel length scales leads to the dominance of viscous forces and reversible motion. Thus, mixing must rely on slow lateral diffusion across the parallel channel streams. However, acoustic microstreaming in microfluidic devices is often used as a means to disrupt the parallel laminar flows seen at the micro-scale for purposes including mixing [11-13]. An oscillating acoustic input at high enough frequency interacts with certain features in a flow field to generate convective time-averaged net flows across the main streams despite the small scale. It overcomes the dominance of viscous forces by introducing a higher oscillatory Reynolds number related to the oscillatory velocity at high frequency which allows inertial forces to become significant [14, 15].

This group has previously studied the concept of acoustic microstreaming in a microchannel by an oscillating membrane[16, 17]. A schematic diagram of the membrane microstreaming-assisted gas exchange device Is presented in Fig. 1. In this configuration, a blood microchannel is fabricated with a gas-permeable PDMS membrane serving as the bottom wall. When the underside of the membrane is bonded over the edge of a rigid substrate, an acoustic signal sent through that substrate is focused through this edge into a mechanical oscillation of the membrane which drives vortex flows in the fluid field above. Then, when a streamwise blood flow is perfused through the channel, a helical or spiral vortical flow pattern is generated by their superposition. The microfluidic artificial lung is seen as a natural application of this concept due to the free-hanging membrane already being a design requirement. The streaming flows enhance the typically diffusion-limited gas exchange by transporting and mixing fluids in the vertical direction and maintaining a higher concentration gradient between the liquid and gas side channels. This enables larger channel (up to mm scale) sizes than would normally be seen in a microfluidic artificial lung device, reducing the shear experienced by the blood, resulting in larger cross-sectional areas which are less likely to be blocked by coagulation, and allowing for the use of conventional machining instead of microfabrication, lowering fabrication difficulty and cost. Study of the flow field, effects of channel geometry, and initial experiments of gas exchange into water are presented in the previous work [16, 17]. This work focuses on the hemocompatibility of the membrane streaming concept with platelet deposition and coagulation experiments and presents the application of the concept to a gas exchange device for the oxygenation of whole ovine blood.

Methods

Fabrication for Membrane Microstreaming

A base configuration to generate the membrane microstreaming flow is used for platelet deposition and coagulation experiments. The process is presented in Fig. 2(a). Soft lithography is used to create microchannel molds. SU-8 2075 negative photoresist (Kayaku Advanced Materials, USA) is coated onto a Si wafer (University Wafer, USA) at 200-600 µm using a spin coater (WS-650MZ-23NPPB, Laurell Technologies, USA). Two spin coating layers are used for thicknesses above 300 µm. After curing, the wafer is placed in a mask aligner (MA6, Karl Suss, Germany) and exposed to ultraviolet (UV) light in the shape of the microchannel profile. The wafer is then placed in a bath of SU-8 Developer (Kayaku Advanced Materials, USA) until the unexposed area of the photoresist is removed. PDMS (Sylgard™ 184, Dow, USA) is mixed in the standard 10:1 ratio of elastomer base to curing agent and cast over the microchannel mold, then cured in an oven at 90 ˚C for 30 minutes. The casting is cut away from the wafer by a razor blade, and inlet and outlet ports are created with a 1 mm biopsy punch.

PDMS membranes are created by spin coating PDMS mixed in the 10:1 ratio on an Si wafer to a thickness of 20 µm, then curing in an oven at 90 ˚C for 30 minutes. The underside of the microchannel casting is chemically bonded by exposing each surface to air plasma using a handheld corona plasma generator (BD-20, Electro-Technic Products, USA) for 1 minute, then placing them together. The casting with bonded membrane is cut away from the Si wafer with a razor blade. The underside of the membrane is bonded over the edge of a glass slide by the same plasma bonding process. A piezoelectric actuator (ABZ2746B-LW100-R, PUI Audio, USA) is attached to the substrate with epoxy. 23-gauge PTFE tubing is inserted into the inlet and outlet ports.

The microchannel profile is shown in Fig. 2(b). The entrance and exit to this section are angled away so that the inlet and outlet port are situated above the substrate for structural stability. It features a main acoustic streaming section with a width of 1.6 mm. The streaming flows are generated by applying a sine wave voltage signal to the piezoelectric actuator through a function generator (33220A, Agilent, USA) and amplifier (Trek 2100HF, Advanced Energy, USA). An example time-averaged membrane microstreaming flow field as measured by particle image velocimetry (PIV) from the data explored in the authors' previous work ([16]) is presented in Fig 2(c). A system of vortices appears above the oscillating membrane with an axis of rotation parallel to the streamwise direction of the microchannel. The peak velocity appears close to the at the bottom of the primary vortex nearest the substrate edge and scales approximately quadratically with input voltage. This peak velocity was measured close to 50 mm/s for an 18.5 V_{rms} input. When superimposed with a streamwise channel flow from a syringe pump parallel to the axis of rotation, these vortices form helical streamlines along the direction of the streamwise flow (Fig. 2(d)).

For gas exchange experiments, the fabrication process is expanded to include a gas channel on the underside of the permeable membrane, shown in Fig. 3(a). The channel with bonded membrane is bonded between separate glass substrates with a gap just wider than the channel width. A flat piece of PDMS is bonded to the underside of the substrates forming a gas channel using the 1 mm height of the substrates as the sidewalls. The exterior is sealed with epoxy, and the Inlet and outlet ports for the gas channel are punched on the outside

View Article Online
DOI: 10.1039/D6LC00360B

of the liquid channel profile. A straight microchannel profile is used, shown in Fig. 3(b) to avoid the microstreaming induced backflow, undesirable for gas exchange as explored in previous work [16].

Platelet Deposition

Platelet deposition experiments are performed as the first measure of the hemocompatibility of the membrane microstreaming concept. Basic microchannel samples are fabricated according to the process described in the previous section. The samples are placed two at a time on a hot plate set so that a small bath of water placed on it reads approximately 37 ˚C. The experimental setup is shown in Fig. 4. A syringe pump (PHD Ultra, Harvard Apparatus, USA) is used to flow Dulbecco's Phosphate-Buffered Saline (DPBS) through the samples at 0.1 mL/min for 10 minutes for pre-cleaning. Then, citrated whole ovine blood is pumped through the channels at 0.1 mL/min for 90 minutes. For each test, one channel is continuously actuated by sending a 5.5 kHz signal at 18 V_{rms} to the piezoelectric actuator while the other sample is left still. Configurations will be denoted ahead by a number representing channel height in microns and a letter to represent actuation status (e. g., 600A for a 600 µm height actuated channel and 250C for a 250 µm height, non-actuated channel). All experiments involving blood samples use whole ovine blood collected by jugular venipuncture using syringes with citrate (0.106 M/L) or heparin (0.5-1.0 IU/mL) as the final anticoagulant concentration. All blood was used within 2 hours post-collection. National Institutes of Health (NIH) guidelines for the care and use of laboratory animals were observed, and all animal procedures were approved by the Institutional Animal Care and Use Committee at the University of Pittsburgh.

After the blood flow, the samples are again cleaned by briefly flowing DPBS through the channels. Then, any deposition on the PDMS surface is fixed by filling the channel with a 2.5% glutaraldehyde solution (Sigma-Aldrich, MO) and letting rest for 2 hr. The PDMS portion of the samples are then cut away from the substrate. Water in the cells is replaced with ethanol to avoid cell collapse during desiccation by submerging the samples in progressively higher concentrations of ethanol in deionized (DI) water solutions (30%, 50%, 70%, 90%, 100%) for 10 minutes each. The samples are desiccated in a vacuum chamber to prepare for scanning electron microscope (SEM, JSM-6330F, USA) imaging. SEM images are captured of the membrane at various positions per sample. Platelet deposition is quantified by an analysis of surface coverage percentage in software ImageJ.

Coagulation and Channel Blockage

Similar experiments are performed to study the effect of the membrane microstreaming on coagulation in the microchannel. The fabrication of the microchannel samples is similar to that in the platelet deposition experiments. In those deposition experiments, some small bubbles precipitated in the channel over time, which led to some minor coagulation at these spots. This is potentially due to the substrates being placed on the hot plate where the microchannel portion hangs off without direct contact, meaning conductive heat transfer into the channel flow must have only occurred through that substrate edge leading to a temperature gradient. This effect occurred similarly regardless of actuation status, and the small affected area was excluded from the platelet coverage analysis so it is not expected to impact those results, but it was important to eliminate the effect for coagulation experiments. For this, the experimental setup was improved with a 3D printed water bath to hold the PDMS portion of the samples in DPBS while keeping the piezoelectric actuators out, also shown in Fig. 4(b). These are placed on a hot plate set so the temperature of the bath is close to 37 ˚C. The channels are precleaned by flowing DPBS at 0.1 mL/min for 10 minutes.

The condition of blood and the nature of the coagulation in the microchannels is highly variable and can change between draws from the donor animal and over time. The anticoagulant condition and performance metrics are therefore adjusted from run to run, and direct comparisons of coagulation is only made between samples which were run side-by-side or immediately following each other. For each blood draw, the concentration of heparin anticoagulant is adjusted (0.5-1.0 IU/mL) in an attempt to induce channel blockage after approximately 30 minutes of blood flow at 0.1 mL/min, though not always successfully. Comparisons are made between channels of differing channel height to examine the effect of increased shear and differing actuation status to examine the effect of the continuous microstreaming flow. For the actuated channels, an 18 V_{rms} sine wave signal at 5.5 kHz is sent to the piezoelectric actuator.

Phase One of this experiment is focused on visualization of coagulation left in the channel after flow. For these tests, blood is pumped through the channel for 40 minutes or until blockage is observed by flow stoppage. DPBS Is briefly pumped through afterwards and the remaining coagulation is observed and categorized qualitatively under an optical microscope. Later, Phase Two of the experiment is focused on continuous quantitative monitoring. A manometer (Dwyer Instruments Inc., Michigan City, IN) is attached to the syringe to monitor the inlet pressure over time until blockage is observed by a rapid increase in pressure or until the sample volume is exhausted. The high range manometer used is not able to measure small variations in inlet pressure due to viscosity increase at the onset of coagulation, but instead detects more extreme increases in pressure due to channel blockage.

Hemolysis

The potential hemolysis effect due to the acoustic waves and streaming flows was analyzed following the Standard Practice for Assessment of Hemolytic Properties of Materials from the American Society for Testing and Materials (ASTM F756-17). Briefly, the blood samples were collected after a blood flow experiment (Fig. 4) for both acoustically actuated and non-actuated channel flow. The collected blood was centrifuged at 750g for 15 min, and 1 mL of supernatant was taken to react with 1.0 mL of Drabkin's reagent for 15 min. The absorbance of the reacted solution was recorded at 540 nm

[18]. The whole blood stored in no additive (Z) tubes was used as a negative control, and the lysis blood using a Triton X solution was used as a positive control [19, 20]. The % hemolysis (hemolytic index) was calculated as: Hemolysis (%) = (haemoglobin concentration in test sample x 100)/ (total haemoglobin concentration). The According to the ASTM F756-17, a material is considered nonhemolytic if the % hemolysis is less than 2%, slightly hemolytic if between 2% and 5% and hemolytic if greater than 5%. PDMS material itself is a biocompatible material (nonhemolytic effect as previously tested [18]).

Gas Exchange

Gas exchange experiments are performed to show the applicability of the membrane microstreaming configuration to the microfluidic artificial lung concept. While the 200 µm and 600 µm channel heights used would normally be too large and unsuitable for microfluidic artificial lung devices due to the lower surface area to volume ratio reducing gas transfer efficiency, the goal is to prove that the addition of active mixing by membrane microstreaming can improve the gas transfer efficiency enough to oxygenate blood to biological levels.

The experimental setup is shown in Fig. 5. Membrane gas exchange samples are fabricated as described previously. The samples are precleaned with DPBS at 0.1 mL/min for 10 minutes. Citrated whole ovine blood is then pumped through the liquid-side channel by a syringe pump at 0.05 or 0.1 mL/min. Oxygen gas is pumped through the gas side channel at 0.2 mL/min by a second syringe pump. For each measurement, 0.15 mL of blood is collected at the outlet of the liquid side, and the partial pressure (pO_2) and saturation (sO_2) among other values are measured by a commercial blood gas analyzer (BGA, Rapidpoint 405, Siemens, USA). The input voltage to the piezoelectric actuator is varied from 0-35 V_{rms} at 5.5 kHz while blood flows through the channel. BGA measurements are also taken directly from the blood draw before channel flow for comparison.

Statistical Analysis

Data are presented as mean ± standard deviation. Comparisons between experimental groups were analyzed by two-tailed student's t-test and significance was established with *: $p<0.05$, **: $p<0.01$, and ***: $p<0.001$.

Results and Discussion

Platelet Deposition

Scanning electron micrographs of platelet deposition on the membrane surfaces comparing actuation status are presented in Fig. 6(a) for both the 600A and 600C samples. It is visually clear that many more cells are adhered to the non-actuated sample in a given area compared to the actuated sample. Quantification by Image J analysis confirms an average 22% coverage in the former case and 4.5% ($p < 0.001$) coverage in the latter case on average as seen in Fig. 6(b). These results are not expected to strongly depend on channel height.

The reduction in biofouling by surface deposition due to acoustic actuation benefits the end application of the microfluidic artificial lung in addition to the primary goal of increasing channel heights. Such biofouling may reduce device lifetimes by acting as sites for clot formation or blocking pathways for gas exchange through the porous membrane. The mechanism of the reduced deposition is likely due to the physical oscillation of the membrane making it more difficult for individual cells to adhere, similar to results seen in previous works [21]. Future studies will additionally investigate platelet activation at the blood outlet using biomarkers, like P-selectin expression [22], CD40 ligand [23]). This will help evaluate the effects of piezo-electric actuation on the platelet activation, as downstream complication can still arise from activated platelets.

Coagulation and Channel Blockage

Comparisons of hemocompatibility from the coagulation experiments are only made between samples tested with blood from the same draw and anticoagulant condition. Fig. 7 presents representative data from experimental runs where each of the four sample configurations were tested with blood volume from the same draw and anticoagulant condition (0.85 U/mL Heparin). Images from Phase One (qualitative visualization) in Fig. 7(a) show that the worst case 250C sample led to channel blockage but the best case 600A sample only showed minor streaks. More representative images can be found in Supplementary 1. Quantitative results were obtained by the inlet pressure measurements.

The pressure plots from Phase Two (quantitative pressure monitoring) in Fig. 7(b) show both the non-actuated 250C and 600C samples experienced irreversible blockage due to coagulation. The 250C channel experienced a sharp rise in pressure almost immediately, spiking for a few minutes until falling to a lower, but still elevated level for a time after. This indicates that the channel experienced immediate failure by blockage, but it was partially cleared by the fluid forced through by the syringe pump. The total blockage was again experienced at approximately 25 minutes. The 600C channel, however, did not experience a measurable pressure increase for approximately 30 minutes before failure by channel blockage. In the case of the actuated channels, neither the 250A nor 600A samples experienced a measurable increase in pressure over the 60-minute runtime of the experiment, indicating a favorable performance against coagulation.

Though the highly variable nature of blood samples and coagulation prevents direct comparison of results across different experimental runs and anticoagulant conditions, the coagulation experiments are summarized by tracking the number of experimental runs where one sample significantly outperformed the other. A compendium of each experiment is presented in Supplementary 1. Of the 12 experiments where the actuation status was compared side-by-side, the actuated sample showed favorable results seven times whereas the non-actuated sample was favored two times (three runs were approximately equivalent). These results indicate that the

acoustic streaming resulting from the actuation may reduce coagulation and channel blockage due to the additional flow patterns preventing individual cells from adhering as they are kept in motion.

The 600 µm channel height showed better performance against coagulation compared to the 250 µm case to a lesser degree (of eleven direct comparisons, five favored 600 µm, two favored 250 µm, and four were approximately equivalent). Likely, the difference between the two channel heights tested was not large enough to establish this trend with more significance. Both of these channel heights are around one order of magnitude or more larger than those featured in other artificial lung works, which can be as small as 10 µm [6], where the poorer hemocompatibility is well established due to increased shear and blood-contacting surface [1, 2, 24]. Such low channel heights were not feasible with the channel profile and flow rates featured in this experiment and were thus unavailable for comparison.

Hemolysis

As shown in Fig. 8, the hemolytic index (% of hemolysis) calculated from the blood after channel flow with acoustic actuation (0.93 ± 0.33%) and without actuation (0.79 ± 0.18%) were considered nonhemolytic (< 2%) according to the ASTM F756-17 in addition to the fresh ovine blood without channel flow as a negative control (0.58 ± 0.14%) (The average absorbance reading for the Triton X positive control was 17.7 ± 2.61 (AU) which was set as 100%, compared to the negative control, actuated channel Flow, and non-actuated channel Flow values of 0.103 ± 0.018, 0.166 ± 0.063, and 0.141 ± 0.032, respectively, for an indication of the dynamic range of the test). Though the actuated and non-actuated channel flow samples show slightly higher index than the negative control ($p = 0.026$ ea.), the difference is small in magnitude and remains under the 2% threshold regardless. The difference between actuated and non-actuated channel flow is not significant ($p = 0.44$), indicating that the acoustic actuation had no observable effect on the hemolysis.

Although, there is a hemolysis concern induced by some mechanically circulated devices [25], this test indicates that the shear stress generated by the channel flow is far less than that those mechanical circulation devices due to the low streamwise flow rate (0.1 mL/min) and an increased channel size (250-600 µm), and that any additional shear stress introduced by the acoustic streaming flows is also small enough in comparison that their combination does not pose a concern for hemolysis.

Gas Exchange

Fig. 9 shows the oxygen saturation measurements for different parameter configurations. All cases show a significant increase in oxygen saturation (ΔsO_2) as the input voltage to the piezoelectric actuator is increased to the maximum of 35 V_{rms}, between 2.2 and 2.6x ($p < 0.001$ ea.) compared to the sO_2 value at 0 V_{rms} (non-actuated). The initial sO_2 condition of the blood sample directly from the draw and before channel flow varied between 62% to 70%.

Rated flow (Q) is a metric to evaluate the performance of artificial lung devices [1]. It is defined as the flow rate at which a gas exchange device can oxygenate blood from an sO_2 of 70% to 95%. At 0 V_{rms} input none of the configurations showed sufficient oxygenation to reach the 95% target to support biological needs. A much smaller channel height and adjusted flow rate would have been required as seen in other microfluidic artificial lung works. At 0.05 mL/min blood flow, 0.2 mL/min O_2, and a channel height of 600 µm, the target 25% ΔsO_2 was reached at 35 V_{rms} input to the actuator using a blood sample which measured 68% sO_2 directly from the veinous draw, so this value is used to estimate the rated flow of the device. Scaled by gas transfer area, the value is 2.4 L/min/m^2, and the associated magnitude of O_2 exchange is 40 ml/min/m^2 which compare favorably with other first generation microfluidic artificial lung works despite the much lower surface area to volume ratio as calculated with the area available for gas exchange of 16.7 cm^{-1} [24, 26-28]. Notably, at the 200 µm channel height, the shortest channel tested shows both a lower magnitude of ΔsO_2 and a lower relative increase compared to the 0 V_{rms} measurement.

CO_2 release was not evaluated in this study. To offer a prediction on its performance, the model for gas exchange for the membrane microchannel configuration established in [1] is examined. The details of the calculation may be found in Supplementary 2. There, the effective resistance to O_2 exchange was calculated, assuming that the effective diffusivity of CO_2 in blood changes by the same factor as that for O_2 when actuation is applied. For a representative inlet partial pressure of CO_2 ($P_{CO2,in}$) of 43 mmHg, ΔP_{CO2} is calculated as 1.03 mmHg for the non-actuated case and predicted as 3.18 mmHg for the actuated case, or 7.5% of the total. Although the predicted relative increase in CO_2 release due to actuation of 3.1x is similar to that for oxygenation, the magnitude of gas exchange would still fall short of a clinical need close to 20% [29]. In future work, CO_2 release performance should be validated experimentally and if true, parameter optimization should seek a more appropriate balance between the exchange of both gasses.

The gas transfer experiments show a significant increase in gas transfer efficiency when active mixing is applied to the blood flow via acoustic streaming driven by the oscillating membrane and was consistent across experimental runs with blood draws from different donor animals. This demonstrates applicability to the microfluidic artificial lung concept while favoring larger channel sizes than are typically seen in these devices. These initial tests demonstrate the efficiency increase in a proof-of-concept device design, and the performance of the device may be further improved in future work by optimizing parameters including channel geometry, substrate design for stronger actuation, and flow rates, and should feature a more robust comparison of channel heights. The device should also be improved in future work by scaling up the number of channel branches to increase total throughput, as the throughput of a single-channel design is clearly insufficient to support biological needs. A multi-channel gas exchange device design featuring

membrane streaming tested with DI water has been explored in the previous work [16].

Conclusion

This work presents an investigation on the applicability of acoustic microstreaming by membrane oscillation to the microfluidic artificial lung concept by characterization of hemocompatibility and proof of concept gas transfer experiments. A study on the fluid mechanics of the microstreaming configuration is presented in a previous work [16]. Briefly, a PDMS membrane serving as the bottom wall of a microchannel is bonded over the edge of a rigid substrate so that a portion is free to oscillate. Acoustic energy sent through the substrate is focused through this edge into a mechanical vibration in the membrane, which drives vortex flows in the fluid field above due to the high oscillatory Reynold's number despite small length scales. The concept is naturally suited to the microfluidic artificial lung since a permeable membrane exposed to a gas channel is already a design requirement.

The hemocompatibility of this microstreaming configuration is investigated in platelet deposition, coagulation, and hemolysis characterization experiments. Platelet deposition experiments run side-by-side with ovine blood from the same draw and anticoagulant condition showed 80% lower platelet deposition on the membrane as quantified by surface coverage for an actuated sample compared to the non-actuated case. This is potentially due to the oscillation of the membrane disrupting or preventing cell adhesion to the surface. Coagulation experiments include visual observation of clotting after blood flow and monitoring of inlet pressure to observe channel blockage. In many individual comparisons of channel height and actuation status with equivalent blood conditions, taller heights were slightly favored over shorter channels, and actuated channels were favored over non-actuated channels. Coagulation and resulting channel blockage are reduced due to reduced shear, lower blood-contacting surface area, and larger cross-sectional area for the taller channel height, an effect which is yet more significant for the shorter channel heights used in typical microfluidic artificial lung works [1, 2, 24]. The additional flow patterns induced by the streaming may also prevent the onset of coagulation due to the improved convection.

A gas exchange device was fabricated to infuse blood with O_2 from a gas channel separated from the blood channel by a permeable PDMS membrane used to generate the microstreaming flow. With the 200 µm and 600 µm channel heights tested, in the case of no membrane oscillation, neither were able to support sufficient gas transfer as measured by sO_2 after the channel flow at the tested flow rate due to the low surface area to volume ratio. Gas transfer was improved up to 2.6x with the strongest oscillation applied to the membrane, reaching a target saturation level to estimate the rated flow of the device to be comparable with other early microfluidic artificial lung works despite the much taller channel height. Further, the taller channel tested showed superior magnitude and relative improvement of gas transfer compared to the shorter channel, allowing the device to capitalize on the associated reduced coagulation and ease of fabrication. Future work may seek to further improve performance by parameter and geometry optimization, as well as investigate scaling up of the device via branching channel designs to increase throughput.

Conflicts of interest

There are no conflicts to declare.

Acknowledgements

This work is in part supported by the NSF (ECCS-2325000) grant.

References

1. Potkay, J.A., *The promise of microfluidic artificial lungs.* Lab on a Chip, 2014. **14**(21): p. 4122-4138.
2. Thompson, A.J., et al., *Design analysis and optimization of a single-layer PDMS microfluidic artificial lung.* IEEE Transactions on Biomedical Engineering, 2018. **66**(4): p. 1082-1093.
3. Astor, T.L. and J.T. Borenstein, *The microfluidic artificial lung: Mimicking nature's blood path design to solve the biocompatibility paradox.* Artificial Organs, 2022. **46**(7): p. 1227-1239.
4. Dabaghi, M., et al., *Microfluidic blood oxygenators with integrated hollow chambers for enhanced air exchange from all four sides.* Journal of Membrane Science, 2020. **596**: p. 117741.
5. Saraei, N., et al., *Scaled-up Microfluidic Lung Assist Device for Artificial Placenta Application with High Gas Exchange Capacity.* ACS Biomaterials Science & Engineering, 2024. **10**(7): p. 4612-4625.
6. Kovach, K., et al., *In vitro evaluation and in vivo demonstration of a biomimetic, hemocompatible, microfluidic artificial lung.* Lab on a Chip, 2015. **15**(5): p. 1366-1375.
7. Barber, R.W. and D.R. Emerson, *Optimal design of microfluidic networks using biologically inspired principles.* Microfluidics and Nanofluidics, 2008. **4**: p. 179-191.
8. Thompson, A.J., et al., *Assessing and improving the biocompatibility of microfluidic artificial lungs.* Acta biomaterialia, 2020. **112**: p. 190-201.
9. Dabaghi, M., et al., *Miniaturization of artificial lungs toward portability.* Advanced Materials Technologies, 2020. **5**(7): p. 2000136.
10. Mercader, A., et al., *PDMS-Zwitterionic Hybrid for Facile, Antifouling Microfluidic Device Fabrication.* Langmuir, 2022. **38**(12): p. 3775-3784.
11. Tan, M.K., L. Yeo, and J. Friend, *Rapid fluid flow and mixing induced in microchannels using surface acoustic waves.* EPL (Europhysics Letters), 2009. **87**(4): p. 47003.
12. Ahmed, D., et al., *A millisecond micromixer via single-bubble-based acoustic streaming.* Lab on a Chip, 2009. **9**(18): p. 2738-2741.

View Article Online
DOI: 10.1039/D6LC00360E

13. Huang, P.-H., et al., *An acoustofluidic micromixer based on oscillating sidewall sharp-edges.* Lab on a Chip, 2013. **13**(19): p. 3847-3852.
14. Sadhal, S., *Acoustofluidics 13: Analysis of acoustic streaming by perturbation methods.* Lab on a Chip, 2012. **12**(13): p. 2292-2300.
15. Wiklund, M., R. Green, and M. Ohlin, *Acoustofluidics 14: Applications of acoustic streaming in microfluidic devices.* Lab on a Chip, 2012. **12**(14): p. 2438-2451.
16. Mercader, A. and S.K. Cho, *Acoustic microstreaming and augmentation of gas exchange using an oscillating membrane towards microfluidic artificial lungs.* Lab on a Chip, 2025. **25**(15): p. 3803-2816.
17. Mercader, A.L. and S.K. Cho. *Strong Microstreaming from a Pinned Oscillating Membrane and Application to Gas Exchange*. in *2023 IEEE 36th International Conference on Micro Electro Mechanical Systems (MEMS)*. 2023. IEEE.
18. Kim, S., et al., *A biostable, anti-fouling zwitterionic polyurethane-urea based on PDMS for use in blood-contacting medical devices.* Journal of materials chemistry B, 2020. **8**(36): p. 8305-8314.
19. Sæbø, I.P., et al., *Optimization of the hemolysis assay for the assessment of cytotoxicity.* International journal of molecular sciences, 2023. **24**(3): p. 2914.
20. Chowdhury, S.M., et al., *In vitro hematological and in vivo vasoactivity assessment of dextran functionalized graphene.* Scientific reports, 2013. **3**(1): p. 2584.
21. Pu, L., et al., *Membrane cleaning strategy via in situ oscillation driven by piezoelectricity.* Journal of Membrane Science, 2021. **638**: p. 119722.
22. Johnson Jr, C.A., et al., *Platelet activation in ovines undergoing sham surgery or implant of the second generation PediaFlow pediatric ventricular assist device.* Artificial organs, 2011. **35**(6): p. 602-613.
23. Yun, S.-H., et al., *Platelet activation: the mechanisms and potential biomarkers.* BioMed research international, 2016. **2016**(1): p. 9060143.
24. Wu, W.-I., et al., *Lung assist device: development of microfluidic oxygenators for preterm infants with respiratory failure.* Lab on a Chip, 2013. **13**(13): p. 2641-2650.
25. Köhne, I., *Haemolysis induced by mechanical circulatory support devices: unsolved problems.* Perfusion, 2020. **35**(6): p. 474-483.
26. Potkay, J.A., *Reply to the 'Comment on "The promise of microfluidic artificial lungs"'by G. Wagner, A. Kaesler, U. Steinseifer, T. Schmitz-Rode and J. Arens, Lab Chip, 2016, 16.* Lab on a Chip, 2016. **16**(7): p. 1274-1277.
27. Hoganson, D.M., et al., *Branched vascular network architecture: a new approach to lung assist device technology.* The Journal of thoracic and cardiovascular surgery, 2010. **140**(5): p. 990-995.
28. Kniazeva, T., et al., *Performance and scaling effects in a multilayer microfluidic extracorporeal lung oxygenation device.* Lab on a Chip, 2012. **12**(9): p. 1686-1695.
29. Hoganson, D.M., et al., *Lung assist device technology with physiologic blood flow developed on a tissue engineered scaffold platform.* Lab on a Chip, 2011. **11**(4): p. 700-707.

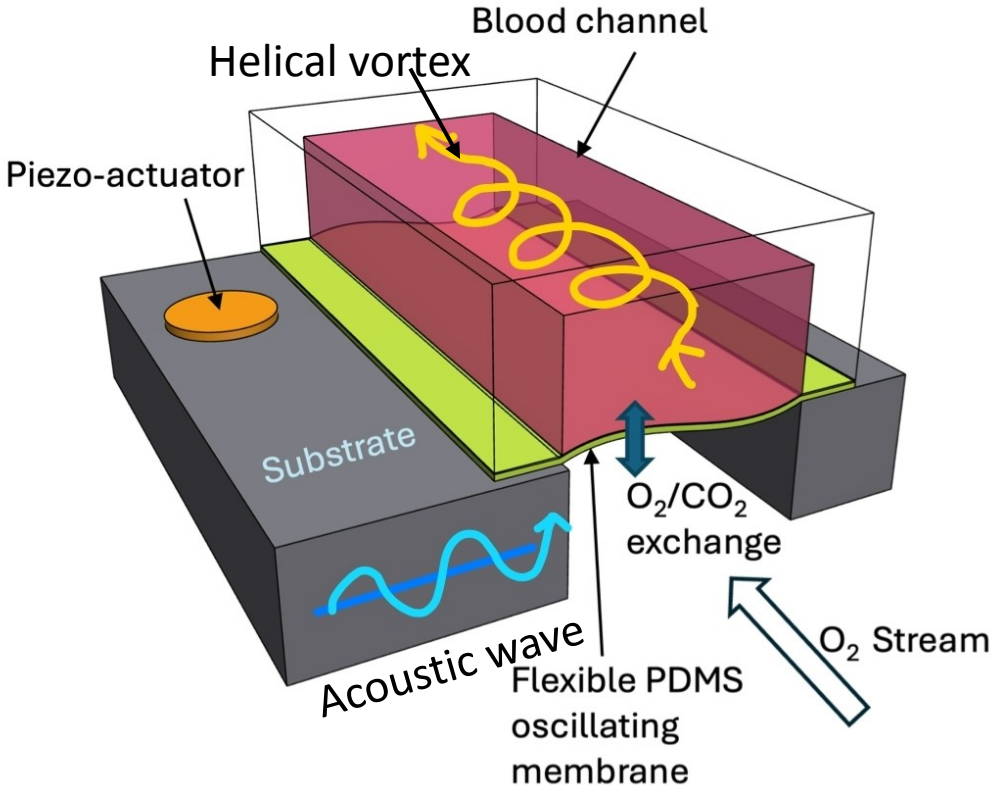

Figure 1: Concept of membrane microstreaming for improved gas transfer efficiency in a microcha

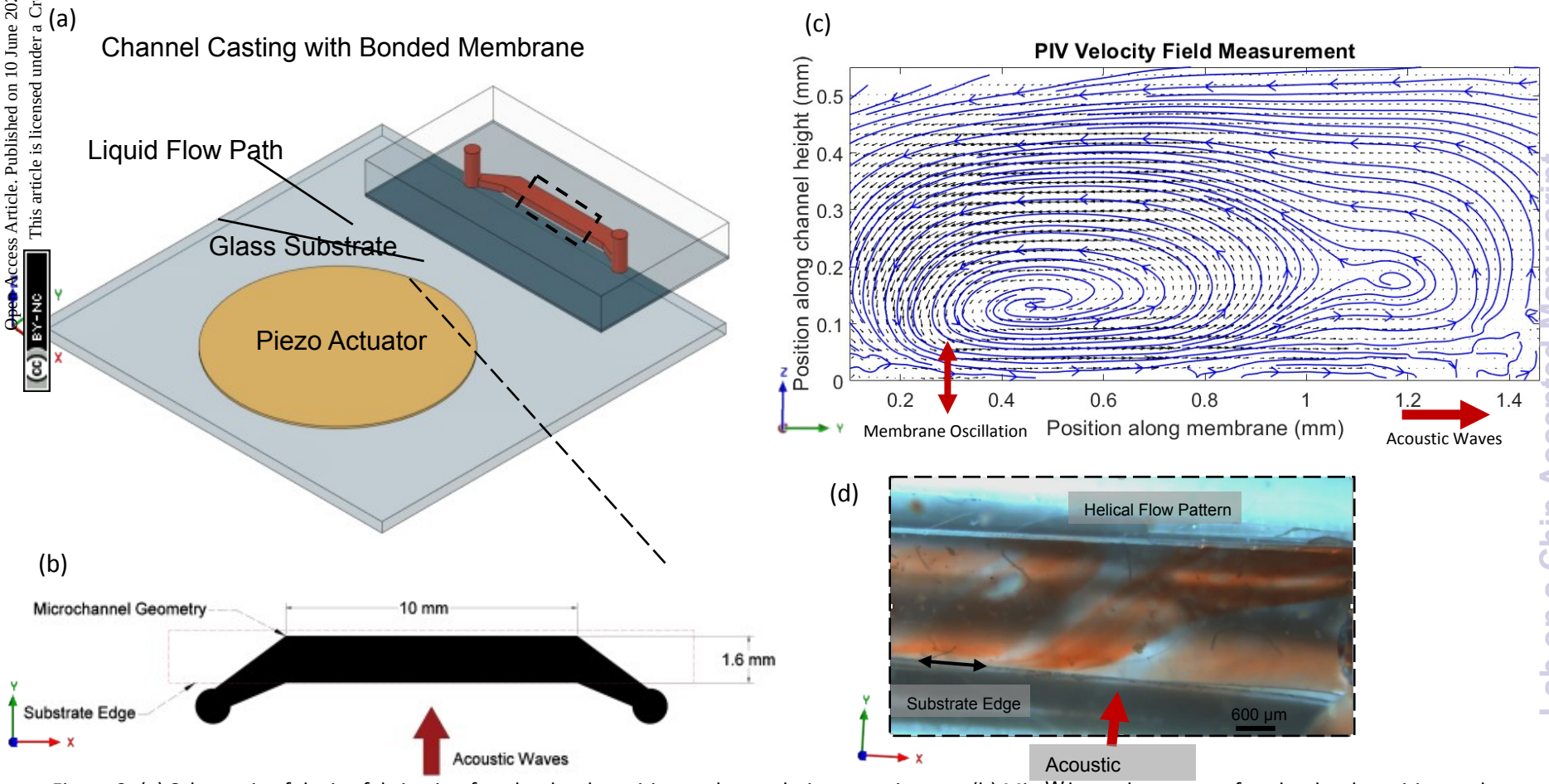

Figure 2: (a) Schematic of device fabrication for platelet deposition and coagulation experiments. (b) Microchannel geometry for platelet deposition and coagulation experiments. (c) PIV velocity field measurement of time-averaged membrane microstreaming over channel cross-sectional area, reproduced with data from [16]. (d) Visualization of helical flow pattern in microchannel due to superposition of acoustic streaming and streamwise channel flow via dye mixing, reproduced from [16].

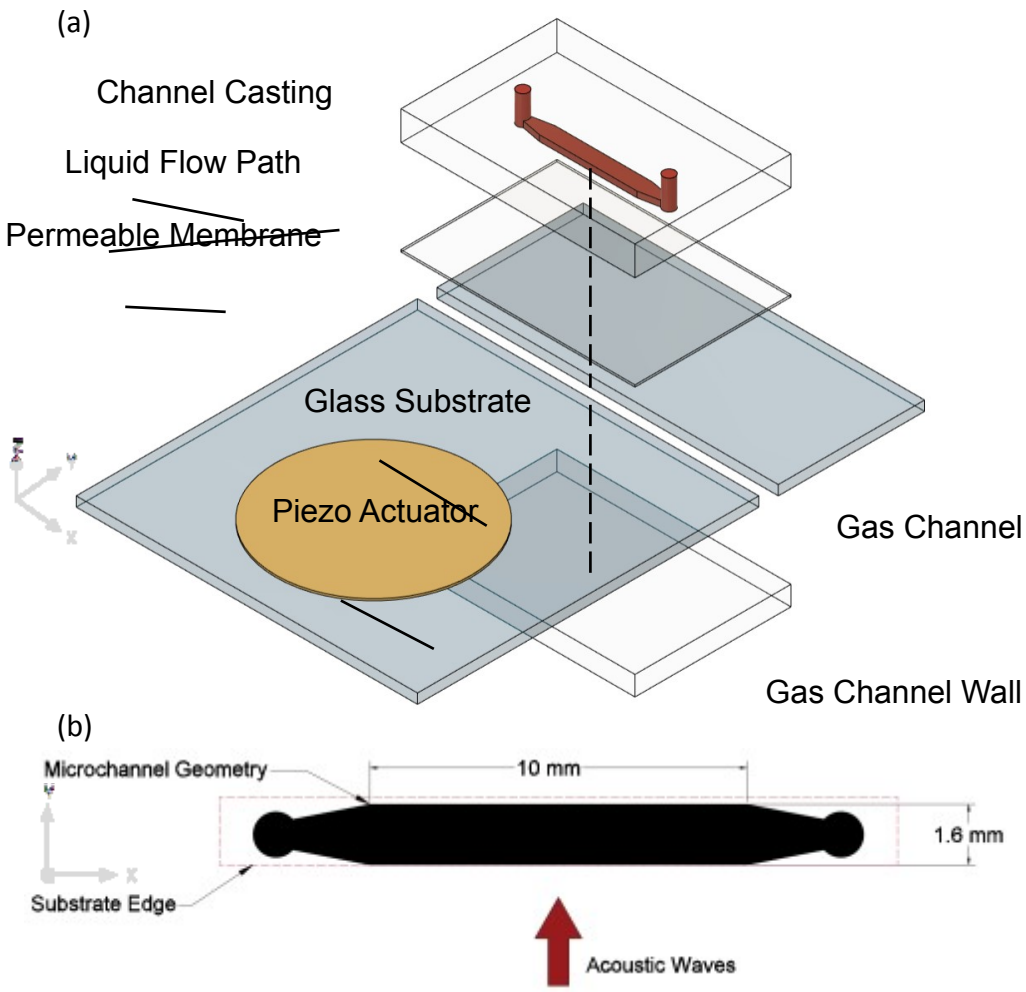

Figure 3: (a) Schematic of device fabrication for gas exchange featuring a gas channel on the underside of the membrane using the substrate as side walls. (b) Microchannel geometry for gas exchange.

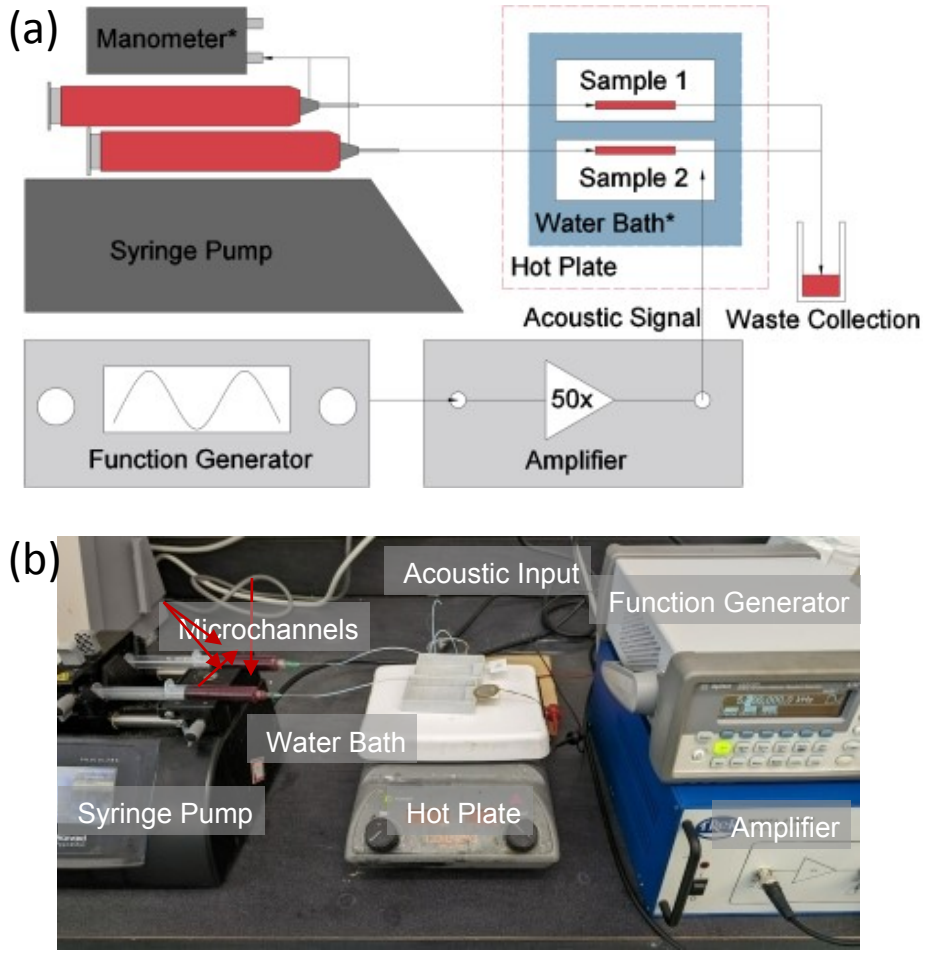

Figure 4: (a) Schematic diagram of blood flow experimental setup for platelet deposition and coagulation tests (b) picture of experimental setup.

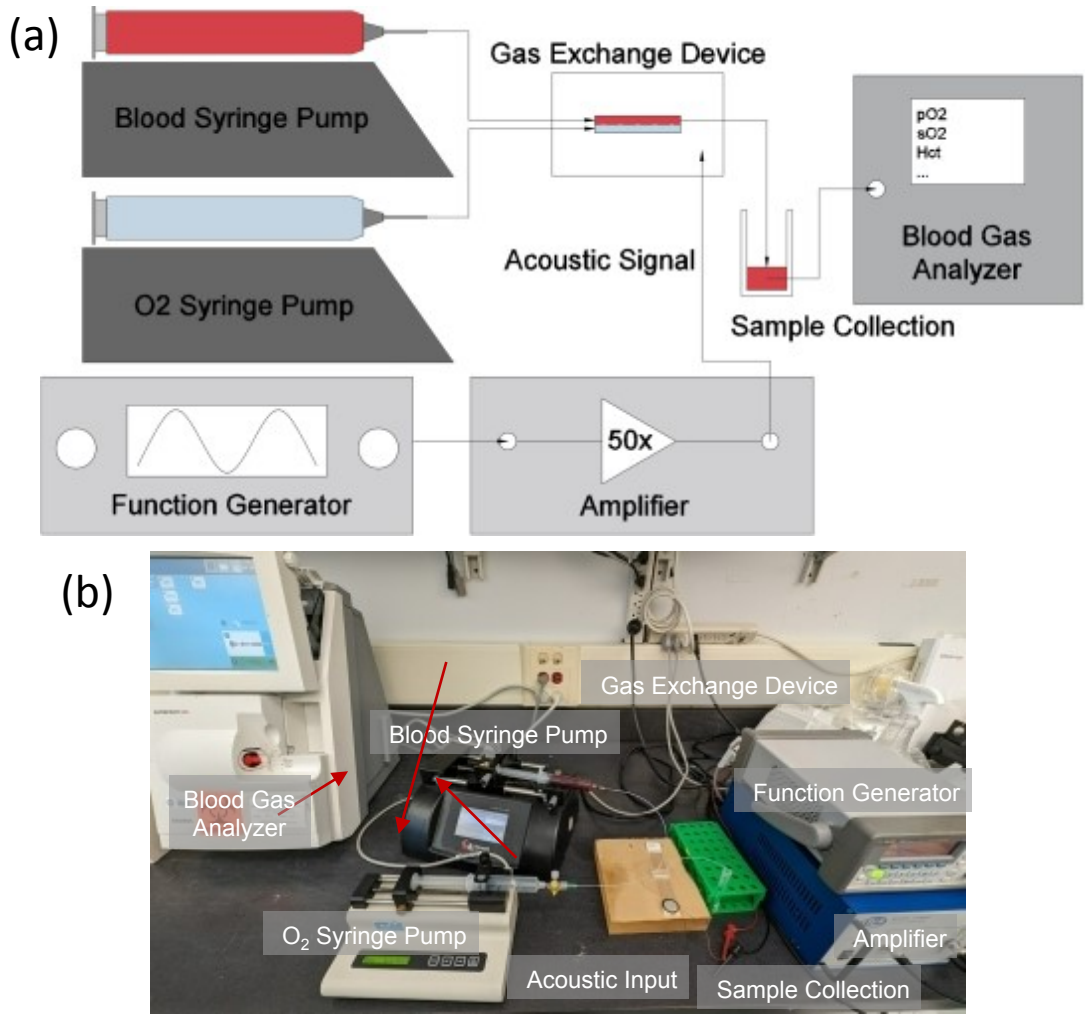

Figure 5: (a) Schematic diagram of blood flow experimental setup for gas transfer tests (b) picture of experimental setup.

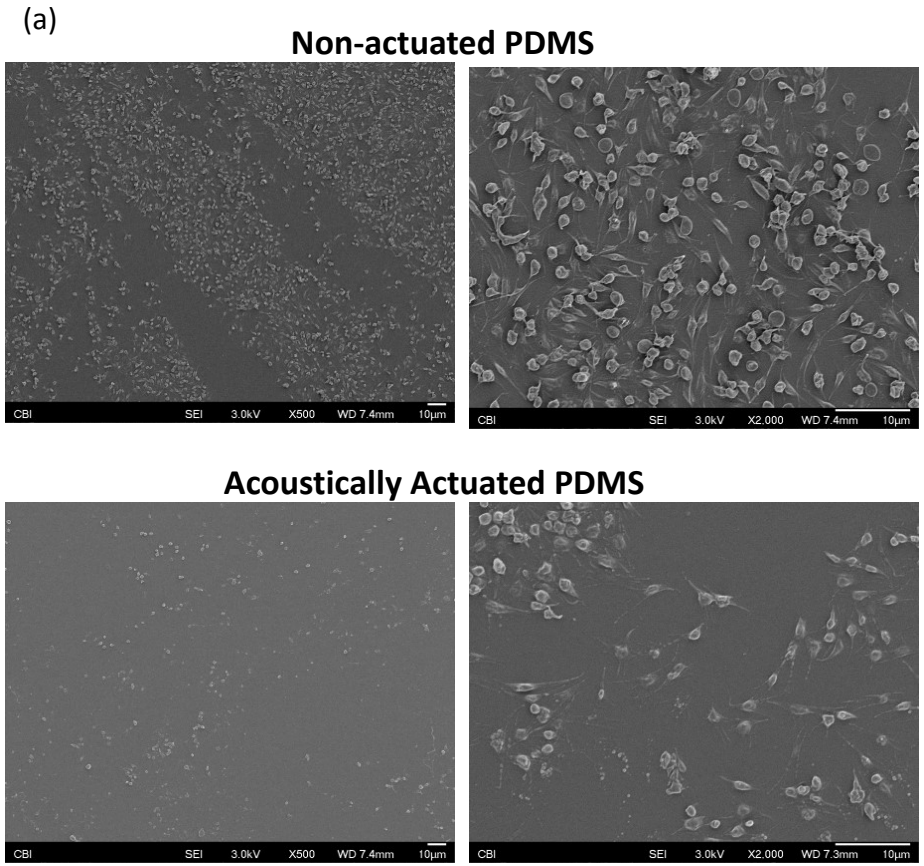

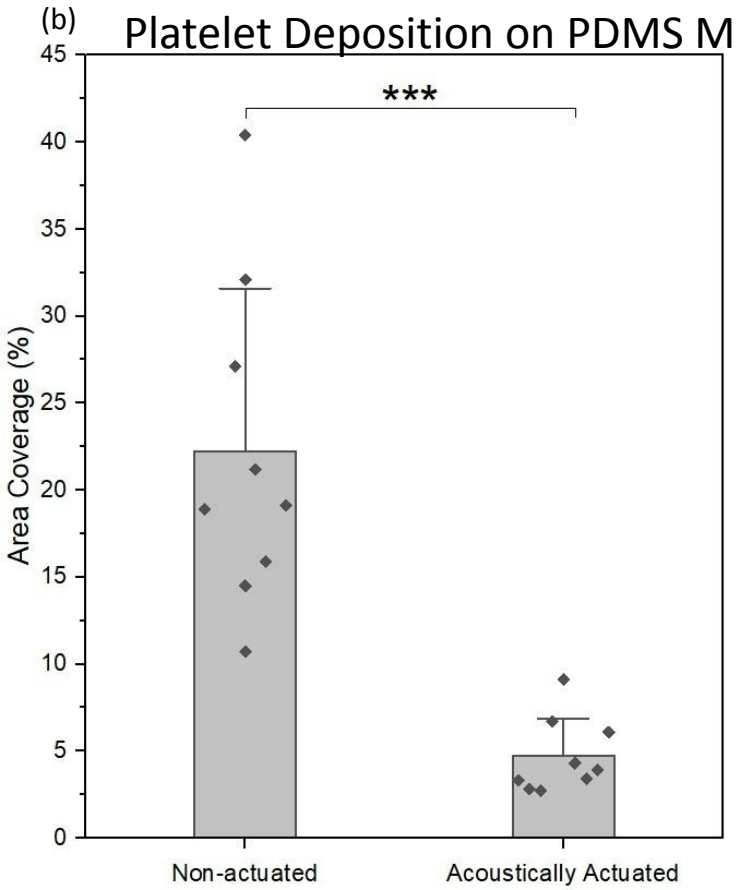

Figure 6: (a) Scanning electron micrographs of PDMS control and actuated PDMS membranes after a continuous blood contact test with fresh ovine blood (citrated) for (scale bars =10 µm). (b) % area coverage of thrombotic deposition calculated by Image J program.

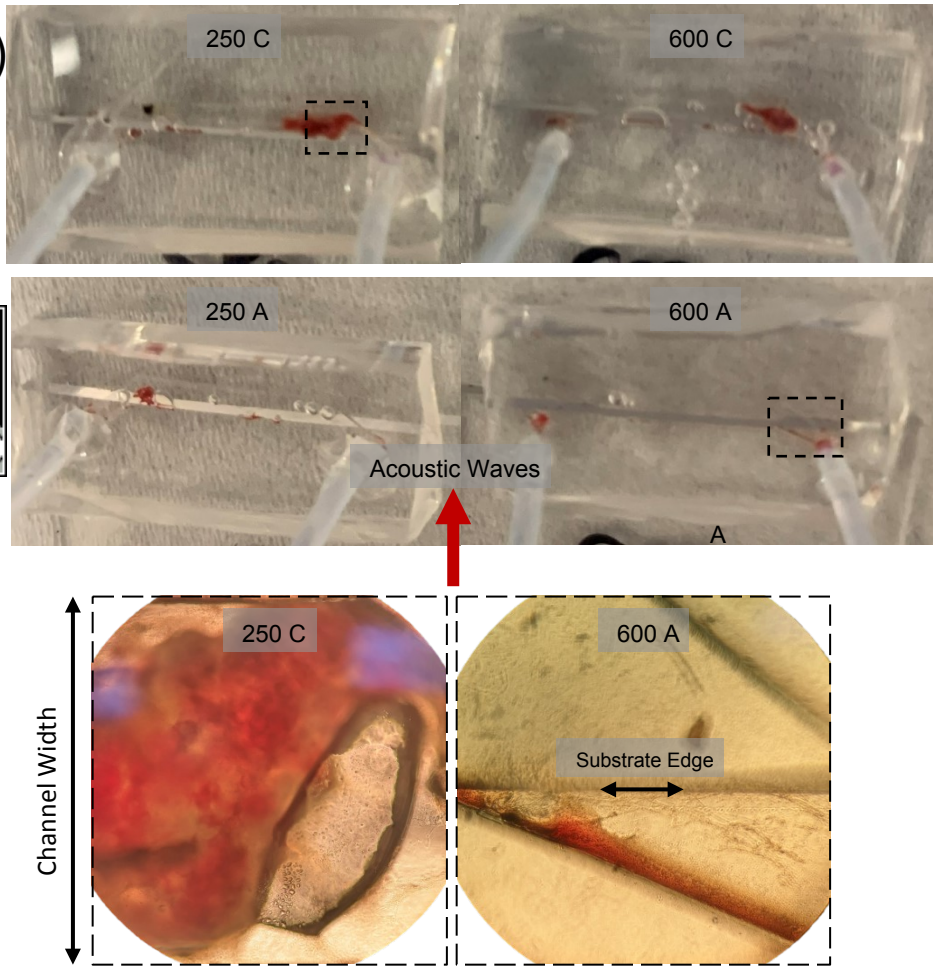

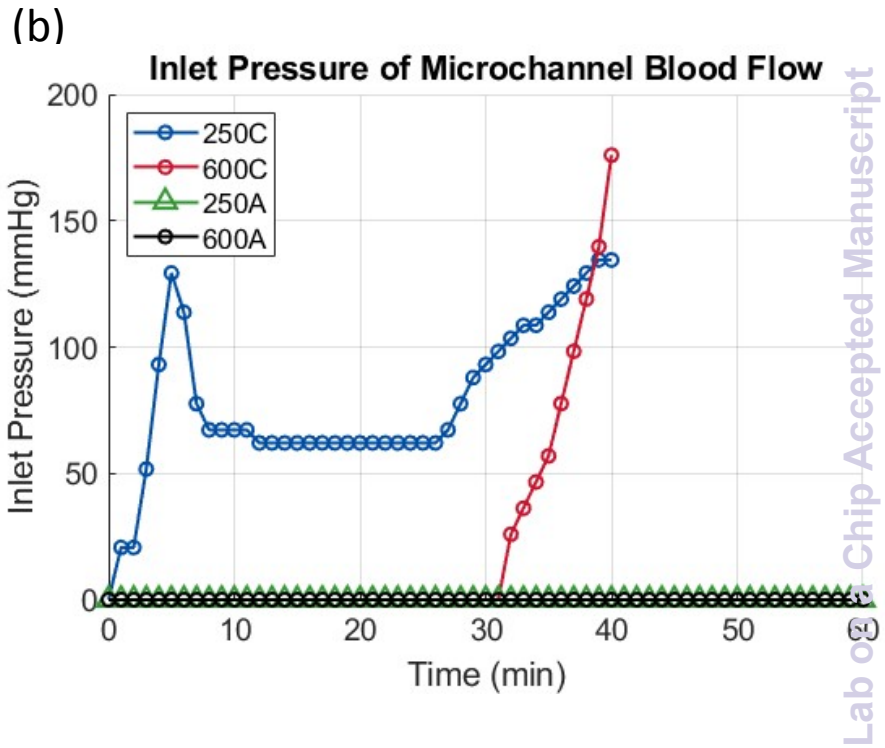

Figure 7: (a) Representative images from Phase one of coagulation experiments (qualitative characterization) of coagulation after channel flow. Total channel blockage observed in 250C sample. (b) Representative plot from Phase two of coagulation experiments (pressure monitoring) showing channel blockage over time in non-actuated samples indicated by increased inlet pressure.

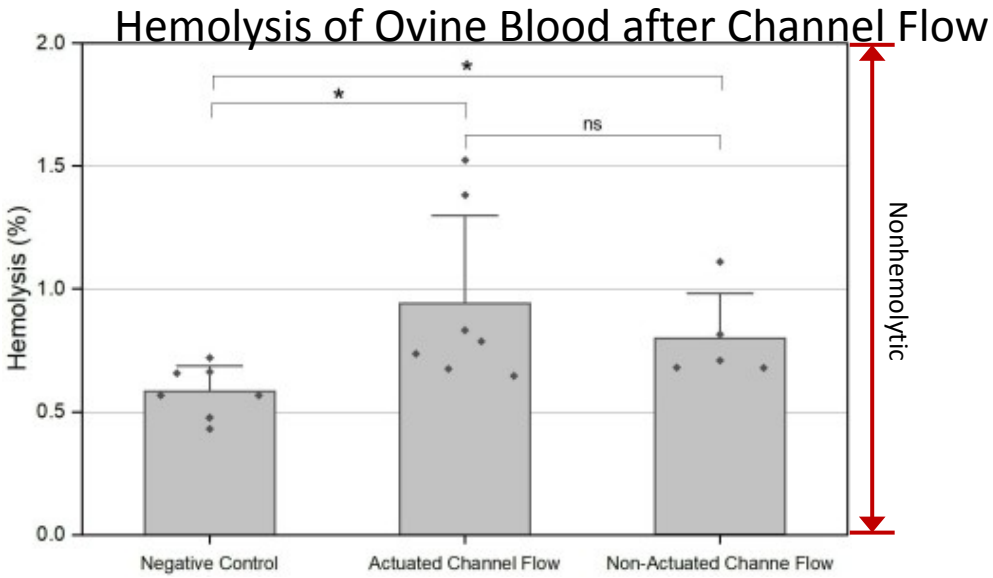

Figure 8: Hemolysis results showing nonhemolytic index (<2%) according to the ASTM standard for the actuated and non-actuated channel flow for ovine blood compared to the negative control.

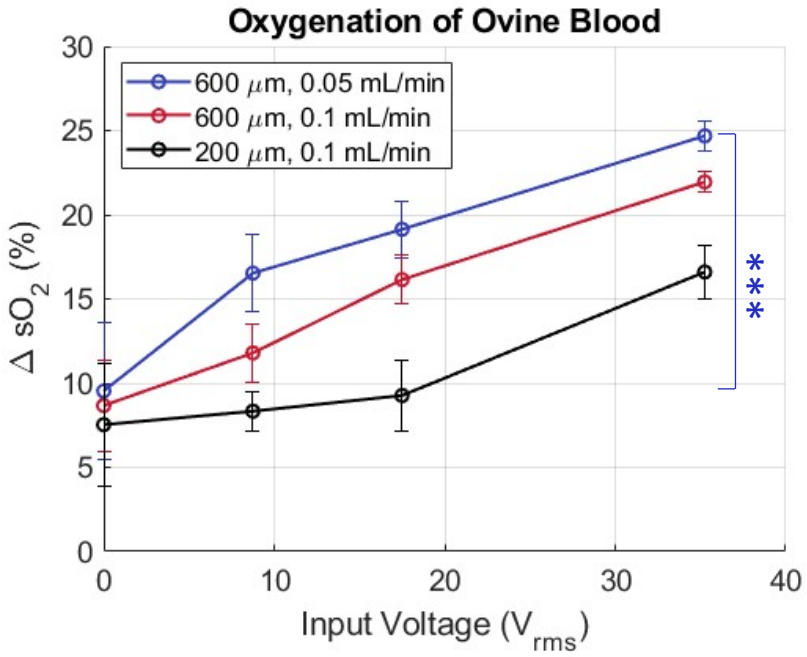

Figure 9: ΔsO_2 plots showing successful augmentation of gas exchange into ovine blood with increasing membrane actuation strength.

View Article Online
DOI: 10.1039/D6LC00360E

Data availability statements

The data that support the findings of this study are available from the corresponding author (Sung Kwon Cho) upon reasonable request